Posterior Malleolar Fracture Patterns

Lukas Mangnus, MD, Diederik T. Meijer, BSc,* Sjoerd A. Stufkens, MD, PhD,*† Jos J. Mellema, MD,*‡ Ernst Ph. Steller, MD, PhD,§ Gino M. M. J. Kerkhoffs, MD, PhD,‖ and Job N. Doornberg, MD, PhD*¶*

Objective: To characterize posterior malleolar fracture morphology using Cole fracture mapping and to study reliability of quantification of 3-dimensional computed tomography (CT)–modeling for posterior malleolar fractures with respect to quantification of fragment size (in cubic millimeter) and true articular involvement (in square millimeter).

Methods: CT scans of a consecutive series of 45 patients with an ankle fracture involving the posterior malleolus were reconstructed to calculate (1) fracture maps, (2) fragment volume, (3) articular surface of the posterior malleolar fragment, (4) articular surface of intact tibia, and (5) articular surface of the medial malleolus by 3 independent observers. Three-dimensional animation of this technique is shown on www.traumaplatform.org.

Results: Fracture mapping revealed (1) a continuous spectrum of posterolateral oriented fracture lines and (2) fragments with posterolateral to posteromedial oriented fracture lines extending into the medial malleolus. Reliability of measurements of the volume and articular surface of posterior malleolar fracture fragments was defined as almost perfect according to the categorical system of Landis (interclass coefficient, range, 0.978–1.000).

Conclusions: Mapping of posterior malleolar fractures revealed a continuous spectrum of Haraguchi III to I fractures and identified Haraguchi type II as a separate pattern. Quantification of 3-dimensional CT–modeling is reliable to assess fracture characteristics of posterior malleolar fracture fragments. Morphology might be more important than posterior malleolar fracture size alone for clinical decision making.

Key Words: posterior malleolar fracture, ankle, Q3DCT

(*J Orthop Trauma* 2015;29:428–435)

INTRODUCTION

To date, fixation of posterior malleolar fractures has been subject of ongoing debate.[1] Current treatment algorithms are based on articular involvement, and advocate operative fixation when 25%–33% of the tibial plafond is involved.[1–5] Limitations of this algorithm include (1) clinical studies evaluate the percentage of articular involvement on plain lateral radiographs with poor reliability[3,6–8] and unknown accuracy as the literature lacks a reference standard; (2) fragment size and articular involvement are hard to determine on lateral views as fracture plane orientation is not parallel to the roentgen beam[9,10]; and finally (3) it has been suggested that 3-dimensional (3D) morphology of the posterior malleolar fragment[10] might be more important than fracture size.[9,11] Correspondingly in elbow fractures, O'Driscoll et al revealed that morphology of a coronoid fracture[12–14] is more important than coronoid fracture height to guide clinical decision making.[15] Three specific types of coronoid fractures are associated strongly with 3 specific overall patterns of traumatic elbow instability.[12,13] In ankle fractures, Haraguchi et al[10] were the first to coin a classification system to categorize posterior malleolar fractures based on fragment pathoanatomy rather than size[10]: type I, posterolateral-oblique; type II, transverse medial-extension; and type III, small-shell fracture. However, clinical relevance of posterior malleolar fragment size, articular involvement, 3D fracture morphology, and correlation to overall ankle fracture pattern have yet to be established.[1]

In this Journal, Cole et al applied 2-dimensional axial fracture mapping to characterize tibial pilon type fractures.[16,17] Cole fracture mapping requires CT models to superimpose 2-dimensional (2D) maps of fracture lines to create a compilation of consecutive cases to identify major and minor fracture lines and therefore define fracture patterns and morphology.[16,17] In addition to this novel technique of fracture mapping, the advent of quantification of 3D computed tomography modeling (Q3DCT) has also been shown valuable to elucidate intraarticular fracture patterns.[18–24] To the best of our knowledge, the Cole fracture mapping technique[17] and

Accepted for publication March 4, 2015.

From the *Orthotrauma Research Center Amsterdam, Academic Medical Center Amsterdam, Amsterdam, the Netherlands; †University of Amsterdam Orthopaedic Residency Program (PGY5), Amsterdam, the Netherlands; ‡Trauma Service, Massachusetts General Hospital, Harvard Medical School, Boston, MA; §Department of Surgery, Sint Lucas Andreas Ziekenhuis, Amsterdam, the Netherlands; ‖Department of Orthopaedic Surgery, Academic Medical Center Amsterdam, Amsterdam, the Netherlands; and ¶University of Amsterdam Orthopaedic Residency Program (PGY4), Amsterdam, the Netherlands.

Presented in part at the eighth Combined Meeting of Orthopaedic Research Societies—CORS, October 13–16, 2013, Venice, Italy, and at the Dutch Annual Trauma Meeting "Traumadagen," November 7–8, 2013, Amsterdam, the Netherlands.

D. Meijer and J. N. Doornberg have received an unrestricted research grant from the Marti-Keuning Eckhart Foundation. The remaining authors report no conflict of interest.

Supplemental digital content is available for this article. Direct URL citations appear in the printed text and are provided in the HTML and PDF versions this article on the journal's Web site (www.jorthotrauma.com).

L. Mangnus and D. Meijer share first authorship based on equal contribution.

Reprints: Job N. Doornberg, MD, PhD, University of Amsterdam Orthopaedic Residency Program (PGY4), Orthotrauma Research Center Amsterdam, Academic Medical Center Amsterdam, G4-Noord, Secretariaat Orthopaedie, Meibergdreef 9, 1100DD Amsterdam, the Netherlands (e-mail: jobdoornbergortho@gmail.com).

Q3DCT-modeling have not been used to date to further characterize and quantify posterior malleolar fractures[18–23] after Haraguchi et al first coined his classification system.[10]

We aim to (1) further characterize posterior malleolar fracture morphology using the novel Cole fracture mapping technique[16,17]; (2) study the reliability of Q3DCT-modeling[18–24] for posterior malleolar fractures with respect to quantification of fragment size (in cubic millimeter) and articular involvement (in square millimeter); and (3) correlate posterior malleolar fracture pathoanatomy as coined by Haraguchi et al[10] to the Cole fracture map as well as to 3DCT quantification of posterior fragment size and articular involvement.[18–24] We hypothesize (1) that Q3DCT is a reproducible technique to measure fragment size and articular involvement; (2) that the posterolateral Haraguchi type I and III fractures are part of a continuous spectrum of oblique fracture lines according to Cole fracture mapping (axial plane) and articular involvement according to Q3DCT-modeling; and (3) that these types I and III differ substantially from Haraguchi type II fractures in terms of fracture line orientation according to fracture mapping, but not significantly with respect to articular involvement according to Q3DCT.

METHODS

Subjects

For this imaging study, a retrospective search was performed for patients with a fracture involving the posterior malleolar fragment between 2005 and 2012 in a Level III trauma center (Sint Lucas Andreas Ziekenhuis, Amsterdam, the Netherlands). Patients were included when they had a fracture involving the posterior malleolar fragment with a complete radiographic documentation including anteroposterior and lateral radiographs, as well as a preoperative CT scan. In this study, we aimed to include rotational type ankle fractures only to characterize and quantify the involved posterior malleolar fragment. Three senior authors evaluated radiographs and CTs independently and distinguished in a consensus agreement between (1) posterior malleolar fractures as part of a rotational type ankle fracture to be included in this study and (2) tibial pilon fractures involving the posterior tibial plafond to be excluded from this study. This resulted in a total of 57 patients; after exclusion of tibial pilon fractures, a group of 45 patients were included in this study. The fractures were classified using the Lauge-Hansen and the Danis–Weber classification systems by 5 authors based on a consensus agreement.[11,25,26] According to the Lauge-Hansen classification,[25,26] the overall ankle fracture patterns of injury were as follows: 26 patients had a supination-external rotation type 4 (SER4) injury (57.8%), 2 patient had supination-external rotation type 3 (SER3) injuries (4.4%), 14 patients had pronation-external rotation type 4 (PER4) injuries (31.1%), and 3 patients had a pronation-abduction type (ProAB 3) injury (6.7%).

The Cole Fracture Mapping Technique

We reproduced the fracture mapping technique as was previously published in this Journal (Fig. 1).[16,17] Selection of a 3D CT view was based on an evaluation of all of the images available, the views that allowed the best visualization of the fracture lines in the plane represented by sagital and axial views of the posterior malleolar fracture were collected for each patient. These views were imported into Macromedia Fireworks MX software (Macromedia, San Francisco, CA) to overlap and orient fracture patterns onto a 3D template image of an intact ankle. Images of each posterior malleolar fracture generated with our Q3DCT-modeling techniques in Rhino were graphically superimposed to create a compilation of fracture planes on a 3D template image of an intact ankle serving as a representation of the osseous anatomy. The overlap of all major fracture planes resulted in a frequency diagram based on the density of fracture planes. Proper rotation and normalization were done by aligning specific ankle landmarks—namely, the medial, lateral, and posterior malleoli, tibia articular surface, and fibula. The template 3D images of intact ankles that we used were axial and sagital views of the right ankle. For superior views of the left ankle, the images were rotated horizontally. Fracture planes created with Q3DCT in Rhino were identified and were traced on top of the combined 3D CT template image of an intact ankle. All mapping was performed by 2 observers (D.M. and J.J.M.) and then was verified by JND and SAS using the original 3D CT rendering. The overlap of the separate fracture planes resulted in a frequency diagram based on the density of fracture lines. This overlapping of all fracture patterns resulted in the creation of an ankle fracture map for posterior malleolar patterns. Zones were defined on the basis of relevant ankle mortise osteology and/or key muscular origins and insertions. With the use of the definitions of relevant zones, all fractures were categorized according to the zones at which they exited the ankle mortise.

Three-Dimensional Modeling Technique

We used the quantitative 3D CT modeling (Q3DCT) technique developed by our 3D laboratory in Boston for quantification and characterization of upper-extremity fractures.[18–24] Digital Imaging and Communications in Medicine (DICOM) is a standard method, which defines the file format and network protocol to exchange data between medical imaging systems (Fig. 2 and www.traumaplatform.org/Q3DCT). The original DICOM files of the CT slices were obtained in a transverse plane. Sagittal planes were thought to result in better accuracy in the 3D reconstruction of the articular surface. The sagittal planes were created by using OsiriX software. OsiriX is a DICOM viewer that can create sagittal DICOM images from the transversal files using multiplanar reconstruction. The sagittal DICOM files had a slice thickness of 1.0 mm or less. The DICOM files were exported for further processing into MATLAB 8.0, a numerical computing environment. With MATLAB, the CT slices were converted into regular pictures (bmp, bitmap). MATLAB identified higher densities and highlighted these as points on the CT slide. These points represented the edges of bone. The created regular images and the additional data were then loaded into Rhinoceros 4.0. Rhinoceros is a program that specializes in nonuniform rational B-spline modeling. Nonuniform ration B-spline is used for generating surfaces and is a mathematical

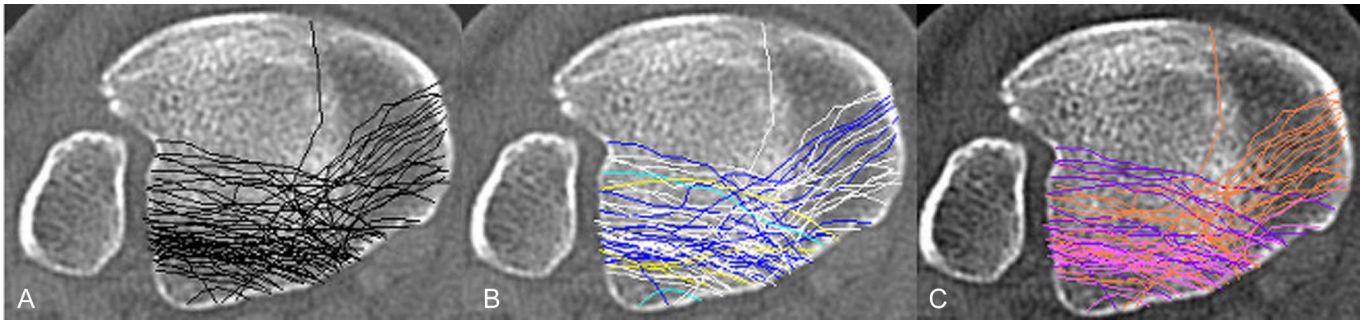

FIGURE 1. The Cole fracture mapping technique[16,17] in a single 2DCT plane 2–3 mm above the articular surface of the tibial plafond as defined in the original article[17]: the posterior malleolar map revealed a fracture pattern and morphology consistent with the fracture lines as originally described by Haraguchi et al[10] in 2D. However, there were basically only 2 deemed major fracture lines: (1) posterolateral-oblique fractures in a continuous spectrum of larger Haraguchi type III fractures to smaller Haraguchi type I avulsion fractures with no apparent cutoff between the 2 types (A). Fracture lines in 2D as classified by Haraguchi in 3D: pink line: type 1, orange line: type II, and purple line: type III (C). We were not able to correlate respective, posterior malleolar fracture pathoanatomy—the Haraguchi classification of posterior malleolar fractures[10] based on Q3DCT—to the Lauge-Hansen overall ankle fracture patterns of injury (white line: supination-external rotation type 4; light blue line: supination-external rotation type 3; dark blue line: pronation-external rotation type 4; and yellow line: pronation-abduction Type) (B).

model commonly used in computer graphics. The images and the additional data were than stacked in rhinoceros taking in account the slice thickness. The points that were created by MATLAB were manually checked and corrected if necessary so that these were correctly placed on the edges of the bone structures and the fragments. From these points, the software drew lines that created a wire model. This wire model could then be used to form a 3D mesh that represented the surface of the cortical bone and the individual fragments.

After creating the 3D models, the articular surface was determined by the investigators (D.M., L.M., J.J.M.). The meshes that represented the articular surface had to be isolated from the tibia and fragments. This was done by drawing a polyline on the articular edge. The edges of the articular surface were determined on the meshes. The meshes that represented the articular surface were isolated from the rest of the tibia and measured. The same technique was used for the volume measurements of the fragments. Surface and volume measurements are standard features in the rhinoceros software. The area of the articular surface was presented in square millimeters, and the volume of the fragments in cubic millimeters. These measurements were preformed on volume of the posterior malleolar fragments and medial malleolus, the articular surfaces of the tibial plafond, posterior malleolar fragments, and the medial malleolus.

To study reliability of Q3DCT-modeling for fragment size and articular involvement of posterior malleolar fractures as described below, 15 patients were selected. To equally represent the different types of fracture, 5 patients were selected per type of fracture as described by Haraguchi et al.[10] Three independent observers reconstructed CT images to Q3DCT-models (D.M., L.M., J.J.M.). All 3 observers

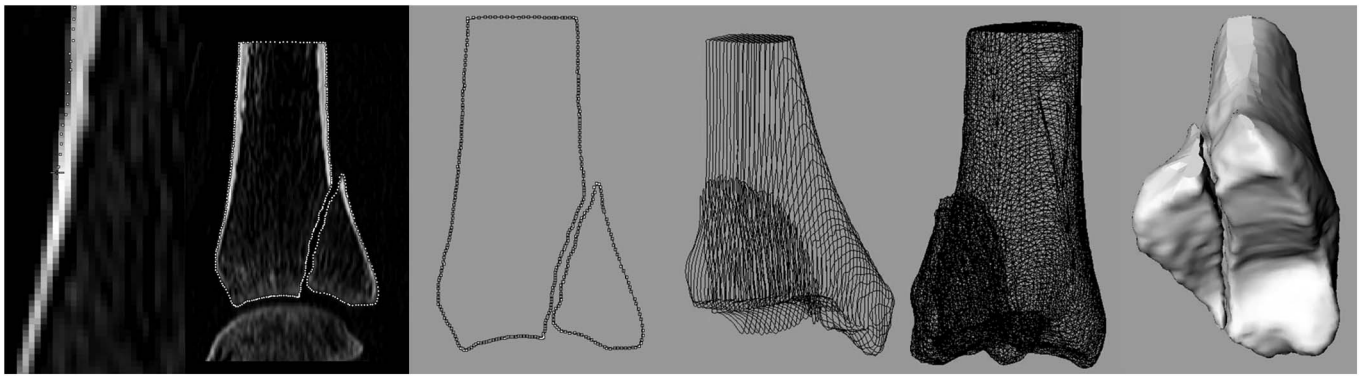

FIGURE 2. We used the quantitative 3D CT modeling technique developed by our 3D laboratory in Boston[24,27] and as illustrated on www.traumaplatform.org/Q3DCT. The original DICOM files of the CT slices were obtained in a transverse plane and converted to the sagittal planes; with MATLAB, the CT slices were converted into regular pictures (bmp). MATLAB identified higher densities and highlighted these as points on the CT slide. These points represented the edges of bone; the created regular images and the additional data were then loaded into Rhinoceros 4.0. The images and the additional data were than stacked in Rhinoceros taking in account the slice thickness; the software drew lines that created a wire model. This wire model could then be used to form a 3D mesh that represented the surface of the cortical bone and the individual fragments; and after creating the 3D models, the articular surface was determined by the investigators.

performed reconstructions and measurements independently. Subsequently, Q3DCT-modeling technique was applied to all 45 included ankles to quantify fragment size, articular involvement, and fragment morphology.

Statistical Analysis

The analysis of Cole fracture mapping was descriptive. For Q3DCT, the interobserver reliability was measured with the interclass correlation coefficient (ICC).[28] Statistical analysis was performed with SPSS statistic software. To evaluate the association between the overall pattern of ankle fractures and fractures of the posterior malleolus, Pearson chi-square analysis was used. A 2-tailed P value of less than 0.05 was considered statistically significant. This corresponds to a chi-square test greater than 7.8 (3 *df*) and 12.6 (6 *df*).

RESULTS

The Cole Fracture Mapping Technique

After critically reviewing all superimposed 2D maps of fracture lines and the compilation of consecutive cases, we identified 2 major fracture lines: (1) a continuous spectrum of oblique fracture lines as depicted in 2D at the level of the tibial plafond as defined by Cole et al in their original Pilon Map article (Fig. 1A),[16] from small posterolateral avulsion type fragments (described by Haraguchi et al as type III), to larger posterolateral-oblique type fragments (Haraguchi type I) (Fig. 1B); and (2) transverse fracture lines that extend into the medial malleolus involving the posterior colliculus (Haraguchi type II).

In other words, as defined according to the Cole mapping technique, the identified fracture pattern and morphology are consistent with the fracture lines as described by Haraguchi in 2D (Fig. 1B).[10] However one could argue that there were basically only 2 deemed major fracture lines: (1) posterolateral-oblique fractures in a continuous spectrum of Haraguchi type III fractures to Haraguchi type I fractures, with no apparent cutoff between the 2 types as shown by the posterior malleolar map (Fig. 1); and (2) transverse fractures of the posterior rim of the tibial plafond in 1 or 2 pieces, consistent with Hargauchi type II.

Specifically, in all but 1 patient with posterolateral-oblique fracture lines, the fracture entered the tibiofibular joint in the posterior third of the fibula incisura in 90% of cases (types I and III). Only 10% entered the tibiofibular joint in the middle third of the incisura (as opposed to 87% of tibial pilon type fractures in the Cole Pilon Map[16]). All posterolateral-oblique fractures, by definition, exited posteriorly, and all but 1 transverse fracture of the posterior rim exited in the middle of the medial malleolus, separating the posterior from the anterior colliculus.

As depicted in Figure 1C, there was no significant correlation between the respective types of Haraguchi I to III and the overall pattern of ankle fracture instability with the numbers available ($P > 0.05$). In other words, there was no correlation found between posterior malleolar fracture pathoanatomy and the Lauge-Hansen overall ankle fracture patterns of injury.

Reliability of Q3DCT for Posterior Malleolar Fracture

The ICC of our measurements was 0.993 [confidence interval (CI): 0.990–0.996]. To assess if all measurements had high ICCs, the measurements were subdivided into 2 main categories (volume and articular surface) and further subcategorized into 1 and 3 subgroups. Volume measurements had an ICC of 0.990 (CI: 0.981–0.995). The subgroup that measured the volume of posterior malleolar fracture fragments ranged from 357 to 2904 mm^3 with an ICC of 1.000 (CI: 0.999–1.000). The second main category (articular surface) had an ICC of 0.9997 (CI: 0.9995–0.9998). The articular surface measurements were subdivided into the posterior malleolar fracture, the tibia plafond, and the medial malleolus. Measurements of the articular surface of the posterior malleolar fracture fragment ranged from 25 to 252 mm^2 with an ICC of 0.998 (CI: 0.996–0.999); the articular surface of the intact tibia plafond ranged from 375 to 1124 mm^2 (ICC: 0.998, CI: 0.996–0.999); and the articular surface of the medial malleolus ranged from 79 to 149 mm^2 (ICC: 0.978, CI: 0.978–0.911). All of these measurements can be classified as almost perfect agreement according to Landis and Koch.[28]

Posterior Malleolar Fracture Types and Patterns

Posterior malleolar fragment size, articular involvement, and 3D fragment morphology varied significantly between the Haraguchi fragment fracture types I to III[10] (see **Table I and Graph I**, **Supplemental Digital Content 1**, http://links.lww.com/BOT/A335): type I fractures (posterolateral-oblique) averaged 3667 mm^3 in size (range, 475–7056 mm^3) and 123 mm^2 of involved articular surface (range, 0–252 mm^2); type II fractures (transverse medial-extension) were the largest in size and articular involvement, averaged 5003 mm^3 in size (range, 2122–9798 mm^3) and 153 mm^2 in involved articular surface (range, 28–275 mm^2); and type III (small-shell fracture) were small, averaged 1670 mm^3 in size (range, 63–2882 mm^3) and 52 mm^2 in involved articular surface (range, 0–134 mm^2) (Fig. 1).

The average articular involvement of the posterolateral type I fractures (15%) was significantly larger than the average articular surface of the posterolateral "shell" type III fractures (5%) (Table 1), although ranges of involved articular surfaces overlap (see **Graph I**, **Supplemental Digital Content 1**, http://links.lww.com/BOT/A335), and Cole fracture mapping reveals a continuous spectrum of fracture lines (Fig. 1).

DISCUSSION

Results of this study support the use of Q3DCT as a reliable reference standard to quantify posterior malleolar fragment size (in cubic millimeter) and articular involvement (in square millimeter). Posterior malleolar fracture patterns—as qualified in the axial plane using the novel Cole fracture mapping technique as described for tibial plafond fractures in this Journal[16,17]—reveal (1) posterior malleolar fragments in a continuous spectrum of posterolateral oriented fracture lines, and (2) fragments with posterolateral to posteromedial oriented fracture lines extending into the medial malleolus.[29,30]

TABLE 1. Qualification and Quantification of Posterior Malleolar Fractures

Haraguchi type based on Q3DCT	Type I				Type II				Type III			
Original descriptive pathanatomy 2DCT	Posterolateral-oblique (N = 13)				Transverse medial-extension (N = 15)				Small shell fracture (N = 17)			
Lauge-Hansen type*	Sup EX 3	Sup EX 4	Pro EX 4	Pro AB 3	Sup EX 3	Sup EX 4	Pro EX 4	Pro AB 3	Sup EX 3	Sup EX 4	Pro EX 4	Pro AB 3
	n = 1	n = 6	n = 5	n = 1	n = 0	n = 10	n = 5	n = 0	n = 1	n = 10	n = 4	n = 2
	7.7%	46.2%	38.4%	7.7%	0%	66.6%	33.3%	0%	5.9%	58.8%	23.5%	11.8%

Quantification	**Average Size**	**Range**	**SD**	**Average Size**	**Range**	**SD**	**Average Size**	**Range**	**SD**
Average articular surface of posterior malleolar fragment (mm^2)	123	0–252	88	153	28–275	69	52	0–134	42
Average articular surface of extension medial malleolus (mm^2)	72	0–178	72	44	0–225	74	74	0–185	69
Average volume of posterior malleolar fracture fragment (mm^3)	3667	475–7056	2287	5003	2122–9798	2568	1670	63–2882	886
Average volume of medial malleolar extension fracture fragment (mm^3)	1087	0–3606	1329	931	0–7548	2047	1154	0–4036	1197
Average articular involvement of posterior malleolar Fracture (%)	**15**	**0–34**	**12**	**19**	3–35	**9**	**5**	**0–14**	**4**

This study should be interpreted in the light of limitations of the imaging and reconstruction techniques: (1) CT images do not account for true articular surface; therefore, absolute measurements might differ from magnetic resonance imaging[31] or cadaveric bone,[32] although stated percentages of relative articular involvement are accurate; and (2) although reliable (ICC: 0.993) for quantification of posterior malleolar fractures, Q3DCT-modeling (Fig. 2) is a very time-intensive technique (www.traumaplatform.org/Q3DCT), and therefore not suitable in this form for application in daily practice. For now, the modeling technique is of academic interest to improve our understanding of fracture patterns and morphology.[18–23] Strong points of this research include (1) to the best of our knowledge, this is one of the few studies evaluating pathoanatomy[3,29,30] of posterior malleolar fractures using CT,[10,33] and the first to qualify and quantify these fractures combining advanced novel imaging techniques—the Cole fracture mapping technique[16,17] and Q3DCT-modeling[18–23]; (2) validation of the applied Q3DCT-modeling technique for posterior malleolar fractures, specifically using 3 independent observers, that was originally developed for upper-extremity fractures by our group[24]; and (3) using an even distribution of all 3 posterior malleolar fracture types according to Haraguchi et al[10] so that the applied technique is proven reliable for large fragments with limited articular involvement and small fragments with substantial involvement.

Haraguchi et al[10] previously coined a classification for posterior malleolar fractures based on 3D pathoanatomy. Based on transverse 2DCT fracture morphology analyzed in 2-mm or 3-mm increments from the proximal extent of the fracture line of the posterior malleolus to the inferior border of the lateral malleolus, the authors recognized 3 types: 67% were large posterolateral-oblique (I), 19% medial-extension (II), and 14% were small-shell types (III). In addition, the authors stated that a medial-extension (type II) fracture usually has 2 fragments or extends to the anterior part of the medial malleolus. In this study, qualification and quantification of the Haraguchi classification using Cole fracture mapping[16,17] and Q3DCT,[18–24] respectively reveal that (1) posterolateral oriented large type I and avulsion type III fractures are part of a continuous spectrum of oblique fracture lines in the axial plane with increasing fracture size (in cubic millimeter) and articular involvement (in square millimeter); and (2) that these types I and III differ substantially from Haraguchi type II fractures in fracture line orientation according to fracture mapping, but not significantly with respect to size and articular involvement. In other words, articular involvement of posterior malleolar fracture fragments does not differ significantly between respective Haraguchi type fractures, although fracture line orientation and 3D morphology does. Therefore, we argue that—similar to O'Driscoll's description of coronoid fractures based on morphology rather than size[12–14]—recognition of posterior malleolar fracture patterns is more important than fracture fragment size in decision making. Clinical relevance of posterior malleolar fragment morphology and correlation to overall ankle fracture pattern have yet to be established.[1]

Despite the advent of CT and ongoing controversies regarding posterior malleolar fractures,[9,10] our study is, to the best of our knowledge, the first to quantify 3D pathoanatomy of posterior malleolar fractures using advanced imaging techniques. Based on our qualification (Cole fracture mapping) and quantification (Q3DCT-modeling) study of posterior malleolar fractures, one could argue that dividing posterior malleolar fracture patterns in 2 basic types might be more appealing clinically: posterolateral versus posteromedial types. Posterolateral fragments require investigation of deep deltoid integrity (in cases of intact medial malleolus) to rule out instability. Posteromedial types are intrinsically unstable because of the fractured posterior colliculus with the deep deltoid ligament attached.[34]

The Cole fracture mapping technique[17] suggests a continuous spectrum of increasing articular involvement across all included posterior malleolar fractures (Fig. 1A), using the

well-defined 2D transverse plane in which the authors recently described a basic Y-pattern for fractures of the tibial plafond in this Journal: the Pilon Map.[16] The current algorithm "when 25%–33% of the tibial plafond is involved, the fragment requires direct fixation[1–5]" seems rather arbitrary, especially when considering that measurements are made on plain lateral radiographs, which are highly unreliable.[8] The concept of Regan and Morrey[15] for fixation of coronoid fractures based on size and articular involvement[15] has been used for decades, until O'Driscoll showed us that morphology of a coronoid fracture[12–14] is more important than coronoid fracture height.[15] Advanced imaging techniques improved our understanding of pathoanatomy of posterior malleolar fractures; however, the clinical relevance of the morphology and correlation to the overall ankle fracture pattern has yet to be established.

Haraguchi's medial-extension type II fractures are straightforward to qualify in the Cole fracture map at the level of the tibia plafond and in 3D (Fig. 1A and Fig. 3). However, qualification of a shell-type III fracture and a posterolateral-oblique type I fracture seems to be unreliable, because the cutoff in the 2D transverse plane is highly subjective. In other words, it can be hard to distinguish a posterolateral-oblique fracture from a shell-type fracture based on 2D transverse images (Fig. 4). Moreover, when fractures are color-coded according to their 3DCT qualification after the original description by Haraguchi et al[10] and subsequent quantification, one could question the clinical relevance (Fig. 1B and Fig. 3). Larger fragments (in cubic millimeter) with little articular involvement (square millimeter) may be considered "large" posterolateral-oblique type I fractures when evaluating axial CTs according to Haraguchi—and depicted in the

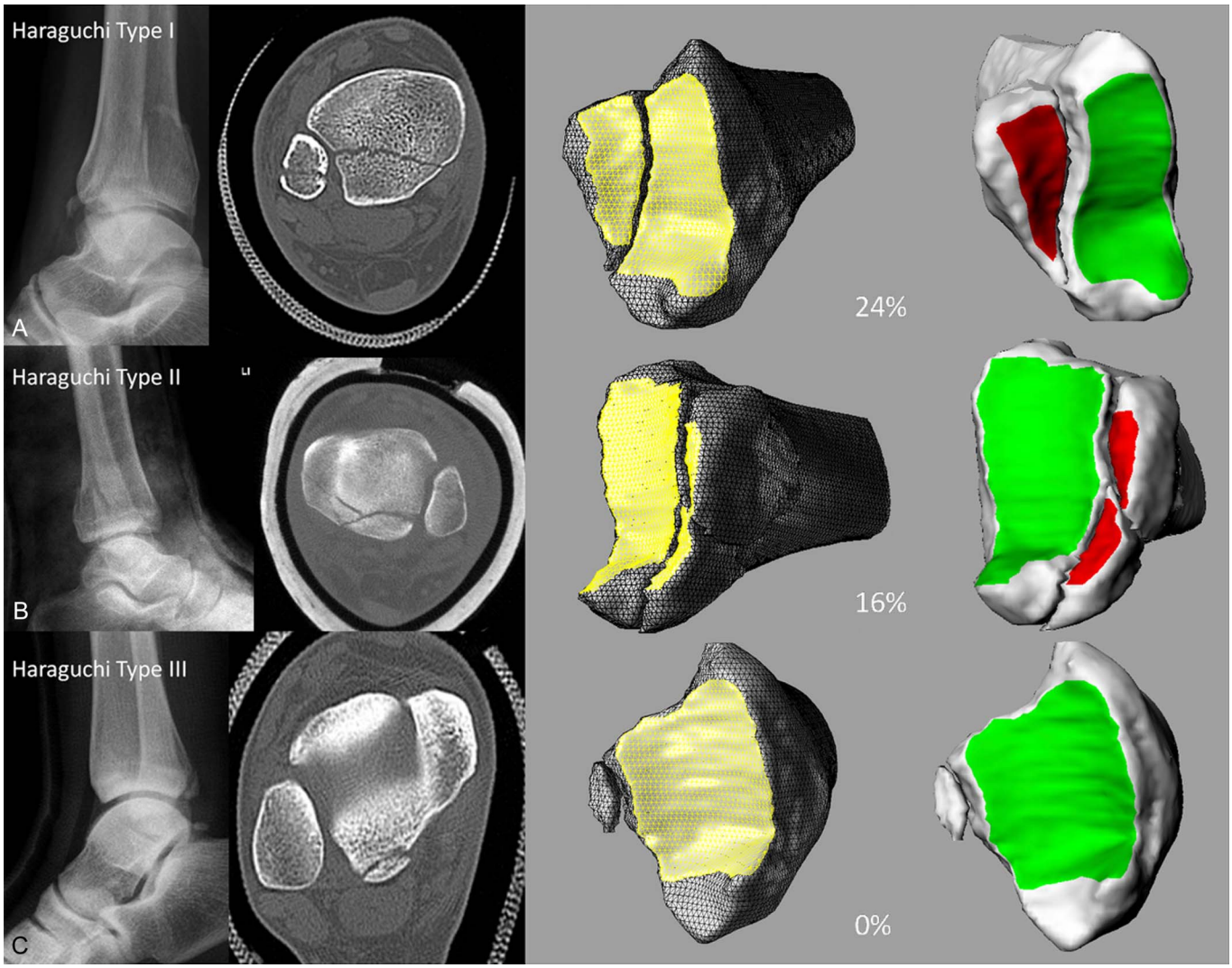

FIGURE 3. Original classification as coined by Haraguchi et al based on transverse 2DCT in 2-mm or 3-mm increments from the proximal extent of the fracture line of the posterior malleolus to the inferior border of the lateral malleolus (9). Posterior malleolar fracture (A) type I, (B) type II, and (C) type III were studied using Q3DCT-modeling (24) to characterize 3D posterior malleolar fracture morphology and to quantify fragment size (in cubic millimeter) and articular involvement (in square millimeter) to correlate to the original Haraguchi classification.

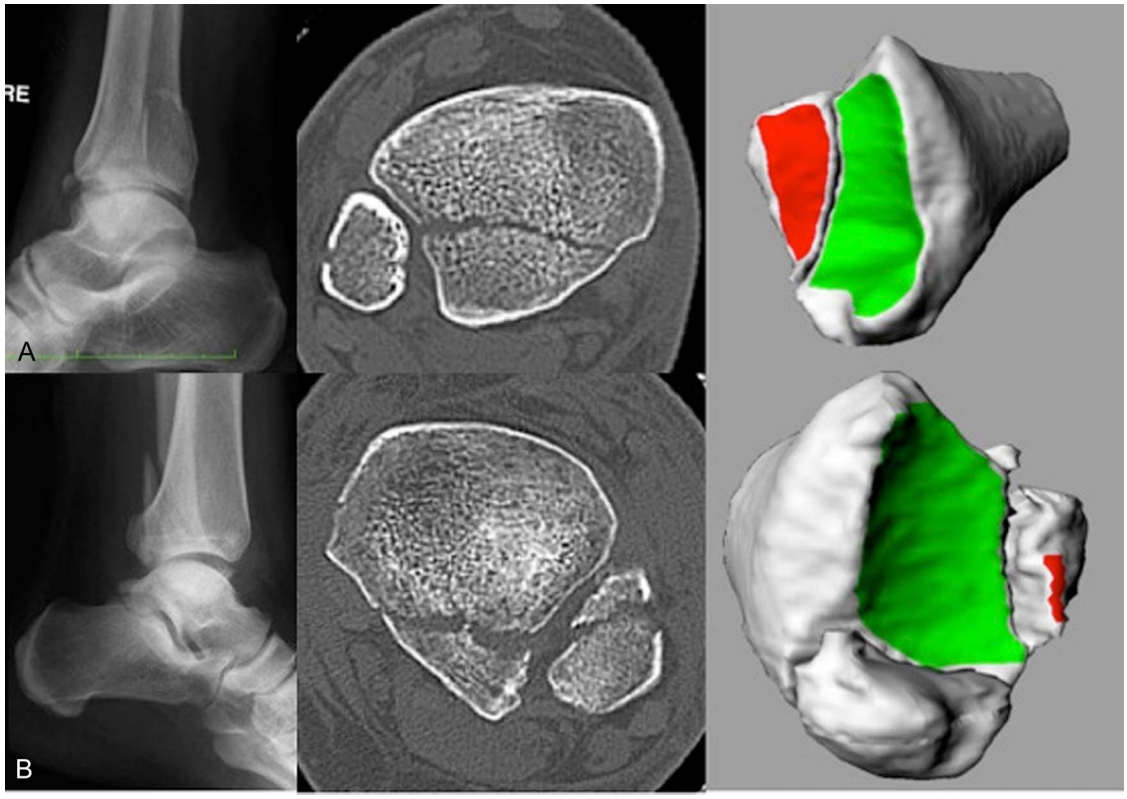

FIGURE 4. Posterolateral-oblique (Haraguchi type I) fracture versus (posterolateral-oblique) shell-type (Haraguchi type III) fracture. (A) Case example of a posterior malleolar fracture with a larger fragment (5301 mm^3) and substantial articular involvement (224 mm^2) that indeed is considered "a large" posterolateral-oblique type I fracture when evaluating an axial CT cut that is 2–3 mm above the articular surface (purple lines in Fig. 1C). (B) Case example of a posterior malleolar fracture with a larger fragment (3750 mm^3) with little articular involvement (38 mm^2) that in 3D appears to be a shell-type fracture (Haraguchi type III) based on limited true articular involvement (3% of tibial plafond). However, one might consider this to be "a large" posterolateral-oblique (Haraguchi type I) fracture when evaluating an axial CT cut that is 2–3 mm above the articular surface (purple lines in Fig. 1C) and based on fragment size.

Cole fracture map—but arguably should be considered shell-type fractures based on limited true articular involvement (in % of tibial plafond) (Fig. 4B), because the "average" posterolateral-oblique type I fractures have substantial articular involvement (in % of tibial plafond) (Fig. 4A).

Future research should return to the basics and focus on long-term clinical outcome of posterior malleolar fractures to identify possible treatment errors. When treatment is based on fragment size alone, long-term outcome of trimalleolar fractures is of only 58% good to excellent.[35] We state that morphology is more important than fragment size. Posterolateral fragments should be inspected for impaction and directly fixed in case of any articular involvement (because it is an intraarticular fracture). Posterolateral shell fragments may be left unreduced in case of medial integrity. One could argue over indirect fixation with syndesmotic screws[36] because the posterior syndesmosis is attached to these shell fragments,[37] but an intact deltoid ligament should keep the talus underneath the tibia leaving no force to diastase the fibula from the tibia.[38,39]

Posteromedial fracture patterns always require a syndesmotic screw, and when possible, direct fixation of the posterior colliculus.[29] In 2004, Weber[29] described a trimalleolar fracture including the posterior malleolar margin: a multifragmentary transverse fracture of the entire posterior tibial lip, including the posterior colliculus of the medial malleolus (as opposed to the more frequently encountered triangular fracture of the posterolateral corner of the tibial plafond). In 2006, Haraguchi et al[10] coined this Haraguchi type II in their CT-based study. Moreover, Weber found intraoperatively that 8 of 9 patients had impacted osteochondral fragments at the posteromedial corner of the tibial plafond that blocked anatomic reduction and allowed posteromedial subluxation of the talus. In our series of 45 rotational type ankle fractures with associated posterior malleolar fractures, 15 were Haraguchi type II (and 30 were triangular fractures of the posterolateral corner of the tibial plafond—in the spectrum of Haraguchi type I and III). Of these 15, the majority (10 of 15) included the impacted osteochondral fragments at the posteromedial corner of the tibial plafond as described by Weber.[29] Poor judgment of this type of fracture (Haraguchi type II), failure to identify the impacted intercalary fragments, and fixation of the posterolateral fragment only might be among the reasons trimalleolar ankle fractures have poor outcomes.[30]

In conclusion, because we came to understand that coronoid fracture morphology and pattern[12] proved more important than "classic" measures of coronoid height,[14] we believe that morphology of the posterior malleolar fragment[10] also might be more important than posterior malleolar fracture size and articular involvement[9] alone for clinical decision making. In ankle fractures, specific fragment morphology could well be associated with overall fracture injury pattern and therefore guide whether or not to fix posterior malleolar fragment.[40] For example, several studies have established the deep deltoid ligament as the primary source of ankle stability.[41–43] Haraguchi type II fractures may be small in size, but because the deep deltoid is attached to the posterior colliculus of the medial malleolus, this fracture type is intrinsically unstable and failure to identify this fracture pattern may lead to poor clinical outcomes and persistent talar subluxation.[29,30,34]

REFERENCES

1. van den Bekerom MP, Haverkamp D, Kloen P. Biomechanical and clinical evaluation of posterior malleolar fractures. A systematic review of the literature. *J Trauma.* 2009;66:279–284.
2. Mingo-Robinet J, Lopez-Duran L, Galeote JE, et al. Ankle fractures with posterior malleolar fragment: management and results. *J Foot Ankle Surg.* 2011;50:141–145.
3. Buchler L, Tannast M, Bonel HM, et al. Reliability of radiologic assessment of the fracture anatomy at the posterior tibial plafond in malleolar fractures. *J Orthop Trauma.* 2009;23:208–212.
4. De Vries J, Struijs PA, Raaymakers EL, et al. Long-term results of the Weber operation for chronic ankle instability: 37 patients followed for 20-30 years. *Acta Orthop.* 2005;76:891–898.
5. Hartford JM, Gorczyca JT, McNamara JL, et al. Tibiotalar contact area. Contribution of posterior malleolus and deltoid ligament. *Clin Orthop Relat Res.* 1995:182–187.
6. Ferries JS, DeCoster TA, Firoozbakhsh KK, et al. Plain radiographic interpretation in trimalleolar ankle fractures poorly assesses posterior fragment size. *J Orthop Trauma.* 1994;8:328–331.
7. Wang L, Shi ZM, Zhang CQ, et al. Trimalleolar fracture with involvement of the entire posterior plafond. *Foot Ankle Int.* 2011;32:774–781.
8. Meijer DT, Doornberg JN, Sierevelt IN, et al. Guesstimation of articular involvement of posterior malleolar fractures -diagnostic accuracy of plain lateral radiographs. In: Association OT, ed. *30th Annual Meeting of the Orthopaedic Trauma Association*. Tampa, Florida: Tampa Convention Center; 2014.
9. Irwin TA, Lien J, Kadakia AR. Posterior malleolus fracture. *J Am Acad Orthop Surg.* 2013;21:32–40.
10. Haraguchi N, Haruyama H, Toga H, et al. Pathoanatomy of posterior malleolar fractures of the ankle. *J Bone Joint Surg Am.* 2006;88:1085–1092.
11. Marsh JL, Slongo TF, Agel J, et al. Fracture and dislocation classification compendium—2007: Orthopaedic Trauma Association classification, database and outcomes committee. *J Orthop Trauma.* 2007;21:S1–S133.
12. Doornberg JN, Ring D. Coronoid fracture patterns. *J Hand Surg Am.* 2006;31:45–52.
13. Doornberg JN, Ring DC. Fracture of the anteromedial facet of the coronoid process. *J Bone Joint Surg Am.* 2006;88:2216–2224.
14. O'Driscoll SW, Jupiter JB, Cohen MS, et al. Difficult elbow fractures: pearls and pitfalls. *Instr Course Lect.* 2003;52:113–134.
15. Regan W, Morrey BF. Fractures of the coronoid process of the ulna. *J Bone Joint Surg Am.* 1990;71A:1348–1354.
16. Cole PA, Mehrle RK, Bhandari M, et al. The pilon map: fracture lines and comminution zones in OTA/AO type 43C3 pilon fractures. *J Orthop Trauma.* 2013;27:e152–e156.
17. Armitage BM, Wijdicks CA, Tarkin IS, et al. Mapping of scapular fractures with three-dimensional computed tomography. *J Bone Joint Surg Am.* 2009;91:2222–2228.
18. Brouwer KM, Bolmers A, Ring D. Quantitative 3-dimensional computed tomography measurement of distal humerus fractures. *J Shoulder Elbow Surg.* 2012;21:977–982.
19. Guitton TG, van der Werf HJ, Ring D. Quantitative measurements of the volume and surface area of the radial head. *J Hand Surg Am.* 2010;35:457–463.
20. ten Berg PW, Mudgal CS, Leibman MI, et al. Quantitative 3-dimensional CT analyses of intramedullary headless screw fixation for metacarpal neck fractures. *J Hand Surg Am.* 2013;38:322–330 e322.
21. Ten Berg P, Ring D. Quantitative 3D-CT anatomy of hamate osteoarticular autograft for reconstruction of the middle phalanx base. *Clin Orthop Relat Res.* 2013;470:3492–3498.
22. van Leeuwen DH, Guitton TG, Lambers K, et al. Quantitative measurement of radial head fracture location. *J Shoulder Elbow Surg.* 2012;21:1013–1017.
23. Doornberg JN, Linzel DS, Zurakowski D, et al. Reference points for radial head prosthesis size. *J Hand Surg Am.* 2006;31:53–57.
24. Guitton TG, van der Werf HJ, Ring D. Quantitative three-dimensional computed tomography measurement of radial head fractures. *J Shoulder Elbow Surg.* 2010;19:973–977.
25. Lauge-Hansen N. Fractures of the ankle: II. Combined experimental-surgical and experimental-roentgenologic investigations. *Arch Surg.* 1950;60:957–985.
26. Yufit P, Seligson D. Malleolar ankle fractures. A guide to evaluation and treatment. *Orthop Trauma.* 2010;24:186–197.
27. Guitton TG, Van Der Werf HJ, Ring D. Quantitative measurements of the coronoid in healthy adult patients. *J Hand Surg Am.* 2011;36:232–237.
28. Landis JR, Koch GG. The measurement of observer agreement for categorical data. *Biometrics*. 1977;33:159–174.
29. Weber M. Trimalleolar fractures with impaction of the posteromedial tibial plafond: implications for talar stability. *Foot Ankle Int.* 2004;25:716–727.
30. Klammer G, Kadakia AR, Joos DA, et al. Posterior pilon fractures: a retrospective case series and proposed classification system. *Foot Ankle Int.* 2013;34:189–199.
31. Matzat SJ, van Tiel J, Gold GE, et al. Quantitative MRI techniques of cartilage composition. *Quant Imaging Med Surg.* 2013;3:162–174.
32. Millington SA, Grabner M, Wozelka R, et al. Quantification of ankle articular cartilage topography and thickness using a high resolution stereophotography system. *Osteoarthritis Cartilage.* 2007;15:205–211.
33. Yao L, Zhang W, Yang G, et al. Morphologic characteristics of the posterior malleolus fragment: a 3-D computer tomography based study. *Arch Orthop Trauma Surg.* 2014;134:389–394. doi: 10.1007/s00402-013-1844-0.
34. Stufkens SA, van den Bekerom MP, Knupp M, et al. The diagnosis and treatment of deltoid ligament lesions in supination-external rotation ankle fractures: a review. *Strategies Trauma Limb Reconstr.* 2012;7:73–85.
35. Stufkens SA, van den Bekerom MP, Kerkhoffs GM, et al. Long-term outcome after 1822 operatively treated ankle fractures: a systematic review of the literature. *Injury*. 2011;42:119–127.
36. van den Bekerom MP, Lamme B, Hogervorst M, et al. Which ankle fractures require syndesmotic stabilization? *J Foot Ankle Surg.* 2007;46:456–463.
37. Zalavras C, Thordarson D. Ankle syndesmotic injury. *J Am Acad Orthop Surg.* 2007;15:330–339.
38. Boden SD, Labropoulos PA, McCowin P, et al. Mechanical considerations for the syndesmosis screw. A cadaver study. *J Bone Joint Surg Am.* 1989;71:1548–1555.
39. Burns WC II, Prakash K, Adelaar R, et al. Tibiotalar joint dynamics: indications for the syndesmotic screw–a cadaver study. *Foot Ankle.* 1993;14:153–158.
40. Michelson JD, Magid D, McHale K. Clinical utility of a stability-based ankle fracture classification system. *J Orthop Trauma.* 2007;21:307–315.
41. Michelson J. Kinematic behavior of the ankle following malleolar fracture repair in a high-fidelity cadaver model. *J Bone Joint Surg Am.* 2002;84A:2029–2038.
42. Sasse M, Nigg BM, Stefanyshyn DJ. Tibiotalar motion–effect of fibular displacement and deltoid ligament transection: in vitro study. *Foot Ankle Int.* 1999;20:733–737.
43. Earll M, Wayne J, Brodrick C, et al. Contribution of the deltoid ligament to ankle joint contact characteristics: a cadaver study. *Foot Ankle Int.* 1996;17:317–324.